Acetylacetone, an Interesting Anchoring Group for ZnO-Based Organic-Inorganic Hybrid Materials: A Combined Experimental and Theoretical Study

ARTICLE *in* LANGMUIR · FEBRUARY 2011

Impact Factor: 4.46 · DOI: 10.1021/la103634v · Source: PubMed

Langmuir

ARTICLE

pubs.acs.org/Langmuir

Acetylacetone, an Interesting Anchoring Group for ZnO-Based Organic−Inorganic Hybrid Materials: A Combined Experimental and Theoretical Study

Tangui Le Bahers,* Thierry Pauporté, Frédéric Labat, Grégory Lefèvre, and Ilaria Ciofini*

LECIME, Laboratoire d'Electrochimie, Chimie des Interfaces et Modélisation pour l'Energie, CNRS UMR-7575, Ecole Nationale Supérieure de Chimie de Paris, Chimie ParisTech, 11 rue P. et M. Curie, 75231 Paris Cedex 05, France

Supporting Information

ABSTRACT: Acetylacetone (**acacH**) adsorption on ZnO (10−10) surface has been studied by a theoretical periodic approach using density functional theory. Two dissociative adsorption modes were investigated and compared to the most stable adsorption mode of formic acid. Acetylacetone appears as a suitable anchoring group for hybrid materials, with adsorption energies of the same order of magnitude as formic acid. IR spectra of the **acac**/ZnO systems were computed in order to determine the spectral signature of adsorption and, possibly, of each adsorption mode to follow the coordination of **acac** on ZnO at the experimental level. The results have been compared to Fourier transform infrared (attenuated total reflection-IR) experimental spectra. The present investigation points out the interest of acetylacetone as an anchoring group for the development of new ZnO-based functionalized hybrid layers for corrosion protection, light emitting diodes, photocatalytic systems, and dye-sensitized solar cells.

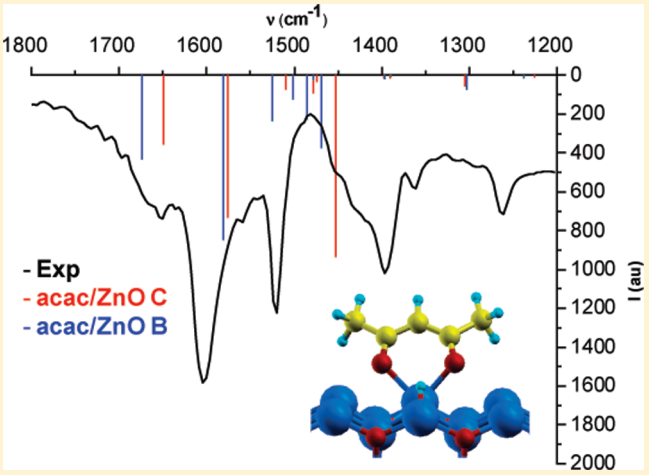

I. INTRODUCTION

An increasing number of new devices and smart surfaces involves the use of hybrid materials made of wide band gap metal oxide semiconductors sensitized by organic or inorganic molecular systems.[1] As typical examples of potential applications of these organic/inorganic hybrid materials and surfaces, we can mention surfaces of switchable wettability,[2,3] dye-sensitized solar cells,[4] corrosion protection,[5] electrochromic films,[6,7] or photocatalytic systems.[8,9]

In order to ensure a high cohesion between the organic and the inorganic parts of such hybrid devices, both from a structural and electronic point of view, chemical anchoring groups are used to link the two subunits. These groups should chemically bind the molecules and the metal oxide surface in order to get robust devices without desorption of the organic molecules from the metal oxide surface. At the same time, the anchoring groups allow for high electronic overlap between the two subsystems granting, for instance, for an efficient interfacial electron transfer in dye-sensitized solar cells.

ZnO has been demonstrated to be a good candidate as semiconductor for new hybrid materials. To better understand the physical origin of technological relevance expected for ZnO-based hybrid materials, it is worth mentioning its wide bandgap energy (3.3 eV at room temperature), good electron conductivity as well as the possibility of obtaining crystallized ZnO in various nanostructured forms.[10,11]

Unfortunately, ZnO is sensitive to the acidic medium created by molecules possessing carboxylic, sulfonic or phosphonic acidic groups. These latter are, indeed, very common anchoring groups used to link the organic/inorganic molecules to the semiconductor surface.[1,7,12]

In the present paper, we address the possibility of using acetylacetone (hereafter noted **acacH** in the neutral form and **acac** in its anionic and adsorbed forms, Figure 1) as an anchoring group to the ZnO surface in hybrid materials. This chemical function possesses several advantages such as a good ability to adsorb on metal oxide surface,[13] an easy synthesis[14] and allows a good electronic overlap between the **acacH** functionalized molecule and the semiconductor surface. For these reasons, **acacH** has been successfully employed for adsorbing both fully organic molecules and metal complexes onto TiO_2 surface in the framework of dye-sensitized solar cells and water photoreduction applications.[15,16]

Received: September 10, 2010
Revised: January 18, 2011
Published: February 22, 2011

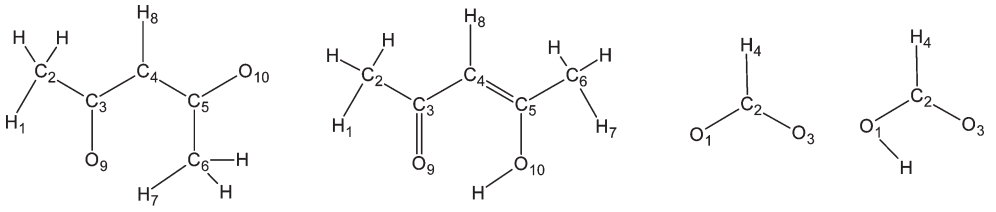

Figure 1. Schematic structures and labeling schemes used for acetylacetonate (**acac**), acetylacetone (**acacH**), formiate (**fa**), and formic acid (**faH**) molecules.

More interestingly, due to its low acidic constant ($pK_a \sim 9$), **acacH** appears as more adapted than carboxylic groups ($pK_a \sim 4$) to be used as anchoring group in ZnO-based hybrid devices.

In order to understand the behavior, at a molecular scale, of this anchoring group on a ZnO surface and compare it to that of carboxylic groups, the geometrical and electronic properties of **acacH** and formic acid (**faH**) adsorbed on ZnO have been studied using a computational approach based on density functional theory under periodic boundary conditions. For the sake of comparison, formic acid (Figure 1) has been also considered here, since it represents the most simple carboxylic type anchoring group.

Calculations give access to both the structural and the energetic features of the adsorption process. As a spectral signature of the adsorption, infrared (IR) spectra of both adsorbed and isolated anchoring groups were computed and compared to experimental data.

The paper is organized as follows. After a detailed description of the computational and experimental protocols applied (section II), results concerning the structural and electronic features of the adsorption are presented and discussed in section III. A detailed analysis of the IR spectral features is also given in the same section and the theoretical results are compared -and confirmed- by the experimental data. Finally, we conclude by the main results concerning the possible use of **acac** as promising anchoring group for ZnO-based hybrid devices (section IV).

II. METHODS

2.1. Computational Approach. All calculations were carried out with the *ab initio* CRYSTAL06 code,[17] making use of localized (Gaussian) basis sets and solving self-consistently Hartree−Fock and Kohn−Sham equations, thus allowing the efficient use of hybrid functionals for band structure calculations.

The most stable crystallographic surface of the wurzite phase of ZnO (that is the (10−10)) was considered for the adsorption of the anchoring groups since this surface is the predominant one for solution-grown ZnO nanostructures.[7,18] Bulk ZnO was first optimized providing the following cell parameters: 3.333 Å (a) and 5.172 Å (c). From that structure a two-dimensional periodic slab[19] was cut out in order to setup a starting slab model for the adsorption, the unit cell being defined by two lattice parameters a and b (the latter corresponding to the c parameter for the bulk) along the ⟨120⟩ and ⟨001⟩ directions, respectively.[20] The slab employed consists of two layers (i.e., four atomic planes).[20] Both the cell parameters and the position of the atoms belonging to the outermost plane were optimized for this ZnO surface. The optimized a and b parameters obtained for this slab model are 3.389 and 5.014 Å, respectively. Clearly, we can notice a significant change compared to corresponding optimized bulk values. These cell parameters were not allowed to further relax upon adsorption of the molecules.

Adsorptions of **acacH** and **faH** were investigated making use of minimal rectangular (4 × 2) and (3 × 2) supercells, corresponding to a surface coverage of one **acacH** molecule per 1.4 nm^2 and one **faH** per 1 nm^2, respectively. Sampling of the irreducible Brillouin zone was done with 1 k point (Γ point) for each system. A detailed investigation of the dependence of various—computed—properties of ZnO supercells as a function of the k point sampling can be found in ref 21.

Organic adsorbates were described using an all electron basis set with 8-411G*, 6-21G*, 5-11G* contractions for O, C, and H atoms, respectively. Durand and Barthelat large core pseudopotential[22,23] with (31/31) contractions were used for O atoms of the ZnO substrate, while large core Hay and Wadt pseudopotentials[24] with (111/111/41) contraction were considered for Zn atoms.

When not specified, calculations were performed at DFT level applying the hybrid exchange correlation functional PBE0.[25] This latter was obtained by casting the PBE correlation and exchange functional[26] in a hybrid HF/DFT scheme, where the HF exchange contribution is fixed a priori to 25%.

This level of theory has already proven to provide reliable geometrical and electronic properties of molecules and periodic systems.[20,21]

During structural optimizations, the adsorbed molecule was allowed to fully relax, as the two outermost atomic planes (i.e., the outermost layer) since surface relaxation of ZnO is known to involve mainly only the outermost planes.[27]

Adsorption energies (E_{ads}) were computed as the difference between the total energies of the combined/adsorbate substrate system and the sum of the relaxed energies of a bare ZnO surface ($E_{surface}$) and of an adsorbate molecule in the gas phase ($E^{vac}_{adsorbate}$) as

$$E_{\mathrm{ads}} = E_{adsorbate/surface} - (E^{vac}_{adsorbate} + E_{surface})$$

Using this notation a negative value of E_{ads} corresponds to thermodynamically favored adsorption process. Adsorption energies were corrected for basis set superposition error (BSSE) using standard counterpoise correction.[28]

Numerical harmonic frequency calculations on periodic systems were performed at the Γ-point on the optimized structures in order to have access to the IR spectra of the adsorbed molecules and the first ZnO layer using the FRAGMENT scheme proposed by CRYSTAL06.[17] Intensities were computed with the Berry phase approach.[29−31] Vibrational frequencies are evaluated at the Γ-point only, since at this point harmonic frequencies can be computed in the same way for both periodic and nonperiodic (molecules) systems.

The same calculations (structural optimizations, IR spectra) were also performed taking into account dispersion forces with the Grimme method[32] as implemented in Crystal09.[33,34] Since the obtained results (geometries, electronic structure and IR spectra) were nearly identical to the ones obtained at PBE0 level, these results will not be discussed in the text but are fully available as Supporting Information.

dx.doi.org/10.1021/la103634v |*Langmuir* 2011, 27, 3442–3450

Analytical frequencies calculations of isolated **acacH** and Zn(**acac**)$_2$ molecules were performed using the Gaussian package[35] and different basis sets namely (i) the small basis (SB) set consisting of the same basis used in Crystal calculations on all atoms but Zn atom, which was always described using a Los Alamos pseudo potential and associated basis set, and (ii) the large basis (LB) set consisting of a 6-311++G(d,p) basis set on all atoms but the metal.

The computed IR spectra of Zn(**acac**)$_2$ with Gaussian and Crystal packages with small basis are practically identical allowing for a direct comparison from Gaussian and Crystal computed vibrational properties.

Effect of anharmonicity were estimated for the free **acacH** using Gaussian09[35] and, for the OH stretching, also using the method implemented in the Crystal09 code.[36,37]

2.2. Experimental. The infrared spectra of isolated **acacH** molecules and **acac** bounded to ZnO were investigated by Fourier transform infrared spectroscopy using the attenuated total reflection (ATR-IR) technique. In the case of the hybrid system, the zinc oxide film was prepared directly on the surface of the ATR diamond crystal (Pike MIRacle). The ATR accessory was a horizontal ZnSe/diamond crystal (A = 3.14 mm^2) with one internal reflection on the upper surface and an incident angle of 45°. An aliquot of 1 μL of a zinc oxide nanocrystal (of about 25 nm in length) suspension (2 g/L in Milli-Q quality water, 18.2 MΩ·cm) was pipetted onto the crystal with subsequent drying under a gentle N_2 flow. This procedure was repeated until a homogeneous layer was deposited. Infrared spectra were measured in a dry air-purged compartment of a Thermo Scientific Nicolet 6700 spectrometer equipped with a mercury cadmium telluride (MCT) detector. The spectral resolution was 8 cm^{-1} and the spectra were averaged over 512 scans.[38]

The reference spectrum consisting of ZnO in contact with ethanol was first recorded since it is known that ethanol adsorbs on the ZnO surface. Then, the ZnO thin layer was sensitized by **acacH** by adding a drop of an ethanolic solution of **acacH** (10^{-3} M) on it. The spectra of adsorbed **acac** on ZnO were recorded when no evolution of the signal was observed (after 15−20 min), assuming that the equilibrium state was reached. It is worth noting that a significant change of the IR spectrum with respect of the reference was recorded thus indicating that **acac** is preferentially adsorbed on the surface. For the solution, the **acacH** IR-ATR spectrum was recorded with an ethanolic solution of **acacH** (10^{-1} M) directly deposited on the diamond crystal.

III. RESULTS

3.1. Insights on Geometrical and Electronic Structure. The adsorption on the ZnO (10−10) surface of formic acid (**faH**), which is considered as the simplest model of carboxylates commonly used as anchoring groups for hybrid materials applications, has been recently studied by different authors using a DFT/periodic approach.[21,39,40] All data in literature support a dissociative adsorption mechanism and a bidentate adsorption mode for **fa** on ZnO(10−10)[21,39,40] consistent with the acidity of this group. Molecules less acidic than **faH**, like methanol ($pK_a \sim 16$) also adsorb dissociatively on ZnO surfaces.[41] Therefore, even if **acacH** is less acid than **faH**, a dissociative mechanism is expected also for this anchoring group. ZnO surfaces are indeed well-known to be very basic (point of zero charge value between 8.7 and 10.3[42]).

In line with the previous studies and due to the structural similarity of the compounds, only two adsorption modes for the **acac** anion on ZnO were analyzed in this study, both of them corresponding to a dissociative adsorption.

The first adsorption mode considered is depicted in Figure 2a and it corresponds to a bidentate mode (hereafter labeled as B) in which each oxygen atoms of **acac** is bound to a different Zn atom of the surface. The second adsorption mode is a chelate mode (noted as C): in this case both oxygen atoms of **acac** are linked to the same surface Zn atom (Figure 2b). This latter is the coordination usually found when **acac** acts as a ligand in coordination compounds (such as Zn(**acac**)$_2$). Different starting adsorption positions were tested for the proton of **acacH** on the ZnO surface. No relevant variations in binding energies, geometries, electronic structures and IR spectra computed for these systems were observed as a function of the proton's position.

The results obtained for the adsorption of **acacH** on ZnO are compared to the features obtained for formic acid on ZnO considered in its most stable conformation that is a bidentate mode (Figure 2c, hereafter B_f) both from a geometrical and energetic point of view.

The most relevant geometrical parameters computed for isolated and adsorbed **acac** are reported in Table 1, along with the structural parameters obtained for the Zn(**acac**)$_2$ complex, here considered as reference for its behavior as chelating ligand in coordination compounds. In the same table the structural data computed at the same level of theory for isolated and adsorbed **faH** are reported for comparison purposes. The Zn(**acac**)$_2$ geometrical parameters are compared to experimental ones obtained by electron diffraction.[43]

Overall, no large change in the internal structural parameters computed for the **acac** molecule is observed going from the isolated to the adsorbed species (for instance variations in bond length smaller than 0.03 Å).

Nevertheless, we notice a sizable increase of the C−O bond when the molecule is adsorbed on the surface compared to its deprotonated free form. The CO bond lengths computed for both the B and C adsorption modes are indeed intermediate between the ketonic (C═O) and alcoholic (C−OH) bond length computed for the free **acacH** and **acac** molecules (Table 1). This fact is per se not surprising and it simply reflects the density depletion of the oxygen atoms due to the formation of Zn−O bonds with the surface. This elongation is in average comparable to the one computed when going from the free **acac** anion to the Zn(**acac**)$_2$ complex (Table 1).

The formation of Zn−O bond is further supported by the computed O−Zn distances which are in the range observed for O−Zn coordination, although slightly longer that the O−Zn distance computed for the Zn(**acac**)$_2$ molecule (Table 1), confirming a chemisorption of the **acac** on the surface.[44,45]

Beside the primary bonding Zn−O interaction between the surface and the **acac** molecule, other—stabilizing—H-bonding interactions are found both in the case of the B and C adsorption modes. The formation of C−H bonds involving the closest H atoms to surface oxygen induces a tilt of the molecule toward the surface but only slightly increases the CH bonds with respect to the isolated **acac**.

Because of the formation of this H-bond network the orientation of **acac** on the surface is different depending on the adsorption mode. For the B adsorption mode, the **acac** slightly leans in the direction ⟨00−1⟩ with a tilt angle of about 43° from the surface. This orientation is analogous to what found in the case of the B_f adsorption mode for **fa** which is found to lean in the same direction but with an angle of 66°. The **acac** is indeed found to be more bent toward the surface than the **fa** in order to maximize the H-bond interaction with the surface oxygen atoms. Also in the case of the C adsorption mode the **acac** is found to be nonorthogonal to the surface but leans, contrary to both the B and B_f modes, along the ⟨001⟩ direction with bending angle of ca. 53°.

dx.doi.org/10.1021/la103634v |*Langmuir* 2011, 27, 3442–3450

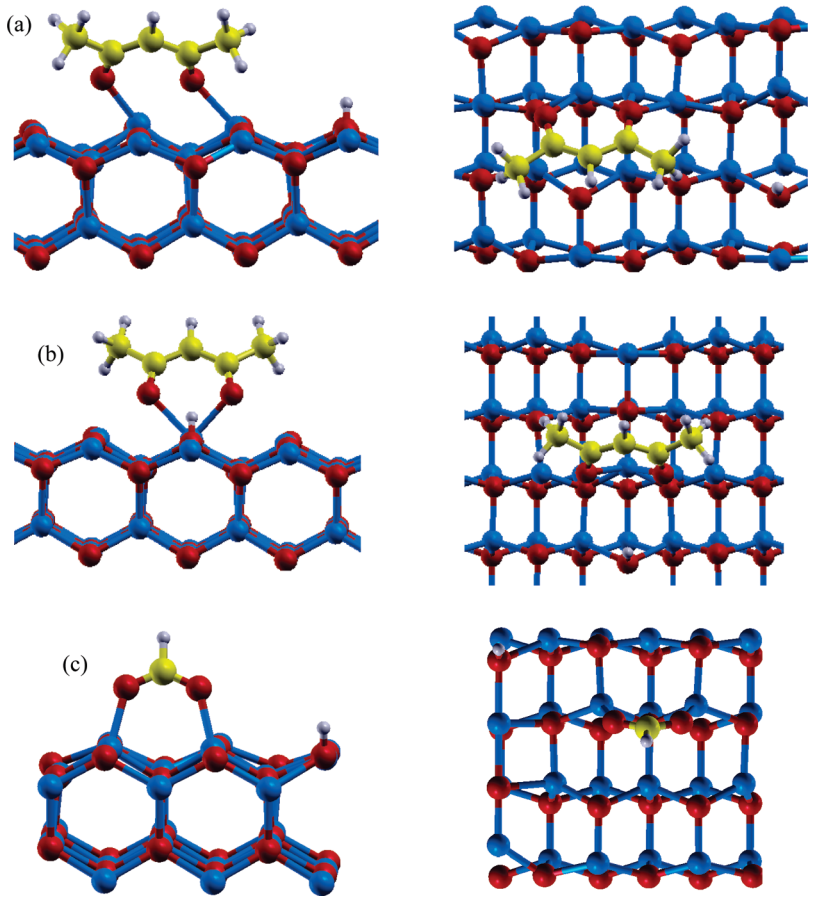

Figure 2. Optimized structures (side view, left; top view, right) corresponding to the bidentate B (a) and the chelate C (b) adsorption modes for **acac** and to the B_f (c) adsorption mode of **fa** on ZnO (10−10) (with their protons adsorbed on the surface). The color scheme adopted is blue, red, yellow, and gray for Zn, O, C, and H atoms, respectively.

As a consequence of the covalent and H-bonds to the surface, from an energetic point of view, the **acac** is expected to strongly adsorb on the ZnO surface. This expectation is indeed confirmed by the adsorption energies computed for both the C and B modes (Table 1). The computed adsorption energies are 126 and 142 kJ/mol, respectively and about half the adsorption energy computed for formic acid at the same level of theory. All the values are an order of magnitude larger than the adsorption energies computed for solvent and additive molecules present in ZnO-based DSCs (all around 20 kJ/mol[46,47]), thus fully justifying the use of **acacH** (and **faH**) as anchoring group in hybrid surfaces and devices. The lateral interaction energies[48] are below 6 kJ/mol for the three systems, which is very weak compared to adsorption energies. This result confirms that the supercells chosen are large enough to avoid lateral interaction between ad-molecules. Effect of dispersion on both geometries and energies of adsorptions, estimated via the Grimme corrections, are found to be negligable and these results are collected in Supporting Information.

The computed adsorption energies are also in good agreement with those reported by Li et al.[49] for the **acacH** adsorption on TiO_2. Indeed, these authors found the B mode to be more stable for the adsorption of **acacH** on a hydroxylated TiO_2 surface.[49] The larger stabilization of the bidentate mode is probably ascribable to the—better—hydrogen bond network created between the **acac** and the ZnO surface which can indeed be strongly perturbed by the presence of coadsorbate molecules (such as solvent or additives) not taken into account in the present theoretical approach.

Considering the electronic structure of the systems, from the analysis of the computed density of states (DOS, Figure 3) we can notice that contrary, to what found for the **faH**[21] which does not modify the electronic structure of ZnO near the Fermi region (i.e., the top of the valence band and the bottom of the conduction band), molecular states are found for **acac** in the Fermi region, both in the case of the B and C adsorption modes.

In particular, a molecular state, centered on the **acac**, is found at the top of the valence band. This state corresponds to a π molecular orbital of the **acac** molecule, with largest contributions centered on the C_2, C_3, C_4, O_9 and O_{10} atoms (see Supporting Informations). As a consequence, the computed gap is reduced upon adsorption of the **acac** molecule going from 3.80 eV (clean ZnO surface) and 3.73 eV (**fa**/ZnO system) to 3.02 and 3.70 eV computed in the case of the B and C adsorption modes for the **acac**/ZnO system, respectively. This effect may be of interest for adjusting the filled molecular level of the system.

Nevertheless, since ZnO is generally used as a n-type semiconductor, the conduction band governs the major electronic properties. Consequently, both the formic acid and the **acacH** are not expected to modify the electronic properties of ZnO as an n-type semiconductor.

Table 1. Selected Geometrical Parameters (Angles in deg, Distances in Å) for Isolated and Adsorbed Molecular Systems and Corresponding BSSE-Corrected Adsorption Energies (in kJ/mol) and Surface Coverage, Θ[a]

			Zn(acac)$_2$			
	acacH	acac[b]	this work	expt[c]	acac/ZnO B	acac/ZnO C
dC_3O_9/dC_5O_{10}	1.322/1.250	1.259/1.254	1.277	1.279	1.279/1.270	1.282/1.279
dC_3C_4/dC_5C_4	1.367/1.435	1.404/1.418	1.401	1.389	1.397/1.404	1.402/1.404
dC_2C_3/dC_6C_5	1.510/1.494	1.539/1.527	1.509	1.504	1.509/1.512	1.506/1.507
dH_1C_2/dH_7C_6	1.093/1.097	1.099/1.097	1.097	1.070	1.103/1.100	1.101/1.100
dC_4H_8	1.085	1.091	1.086	1.060	1.086	1.086
$dO_9Zn_s/dO_{10}Zn_s$	--	--	1.972	1.942	2.164/2.062	2.179/2.109
E_{ads} (BSSE)	--	--	--	--	−142	−126
Θ	--	--	--	--	1/4	1/8

	faH	fa	fa/ZnO B$_f$
dC_2O_1/dC_2O_3	1.216/1.302	1.250/1.250	1.256/1.256
dC_2H_4	1.137	1.148	1.106
dO_1Zn_s/dO_3Zn_s	--	--	2.026/2.025
E_{ads} (BSSE)	--	--	−246
Θ	--	--	1/3

[a] For labeling scheme refer to Figure 1. For comparison the Zn−O distance in the bulk is 1.998 Å (expt) and 2.000 Å (theor) while its mean value is computed to be 1.919 Å for the {10-10} ZnO surface. [b] In *trans* conformation. [c] From ref 43.

3.2. Insights into Vibrational Properties: IR Spectroscopy. From an experimental point of view, vibrational spectroscopies (both IR and Raman) in principle offer a tool to monitor, and also eventually screen, the coordination of the **acac** molecule on ZnO. In fact, one can reasonably expect that, upon coordination on the semiconductor surface the vibrational signature of the **acacH** molecule will change. In particular, we expect that the C−O stretching frequencies will be mostly affected while other bands will appear or disappear.

For these reasons, the IR spectra of the free **acacH** molecule, of the Zn(**acac**)$_2$ complex and of the adsorbed **acac** (both in a bidentate and a chelating mode) were computed and compared to the available experimental data recorded in gas phase[50] and matrix.[44] Influences of anharmonic effect were estimated for the free **acacH** molecule. As expected, only the OH stretching was significantly affected by this correction, a decrease of 480 cm^{-1} being computed. On the other hand, vibrations corresponding to the CC and CO stretching modes are poorly affected by anharmonicity (less than 50 cm^{-1}).

First of all, the IR spectrum computed for the free **acacH** molecule was compared to that of the Zn(**acac**)$_2$ complex here considered as prototype of a chelating coordination (Figure 4). Since accurate experimental data are available for these two systems, these calculations also serve as benchmark of the computational protocol.[44,50] Two different basis set were used: the SB corresponding to the basis set used for periodic calculations and the LB basis corresponding to the more common 6-311++G(d,p) basis for light atoms. In both cases the Zn atom was described by a Los Alamos (LANL2) pseudo potential and corresponding double-ζ valence basis set. The IR frequencies computed for the free **acacH** and the Zn(**acac**)$_2$ molecules using the two above-mentioned basis sets are compared in Supporting Information. From this plot it is clear that basis set effects are practically negligible. In particular, beside the good correlation (R = 0.999) obtained both for **acacH** and Zn(**acac**)$_2$, the slope and the intercept of the linear regression are very close to the value expected for an ideal correlation, that is 1 and 0, respectively.

Next, the IR spectral features of the above-mentioned systems were compared to the data computed for the **acac** adsorbed on the ZnO surface in order to identify possible frequencies that could give a hint about coordination and, eventually, about the coordination mode.

In Table 2, comparison with gas-phase IR data available in the literature[44,50] allows to further validate our computational protocol. Indeed, if in both cases shifts between experimental and computed data are found, relative intensity and position of the main IR bands are well reproduced by calculations. In this respect, we would like to stress that this is the order of magnitude of accuracy that we can reasonably reach with calculations when using a harmonic approximation in gas phase with a limited basis set.

In particular, the characteristic CO and CC stretching occurring in the 1700−1500 cm^{-1} region (reported in Table 2) as well as the enolic (OH) stretching of the **acacH** (computed at 2995 cm^{-1} and experimentally corresponding to a broad band around 2800−2900 cm^{-1})[50] are correctly reproduced by our calculations. Therefore, the computed shift between **acacH** and Zn(**acac**)$_2$ can be considered as reasonable indicators of **acac** coordination.

Although most of the frequencies computed for the free **acacH** are relatively close to those of the Zn(**acac**)$_2$ complex, and thus cannot be used to monitor its formation, three main features can be noticed in Figure 4: (1) the band computed at 3000 cm^{-1} for the free **acacH** is absent in the complex; (2) a new transition, at ca. 500 cm^{-1} is present in the case of the Zn(**acac**)$_2$ complex; (3) there is a clear shift going from **acacH** to Zn(**acac**)$_2$ of the two most intense bands computed at ca. 1700−1500 cm^{-1}.

The disappearance of the band at 3000 cm^{-1}, corresponding to the stretching of the hydroxyl OH bond, can be hardly used to monitor the formation of a complex since this band is experimentally very broad and following its evolution upon complex

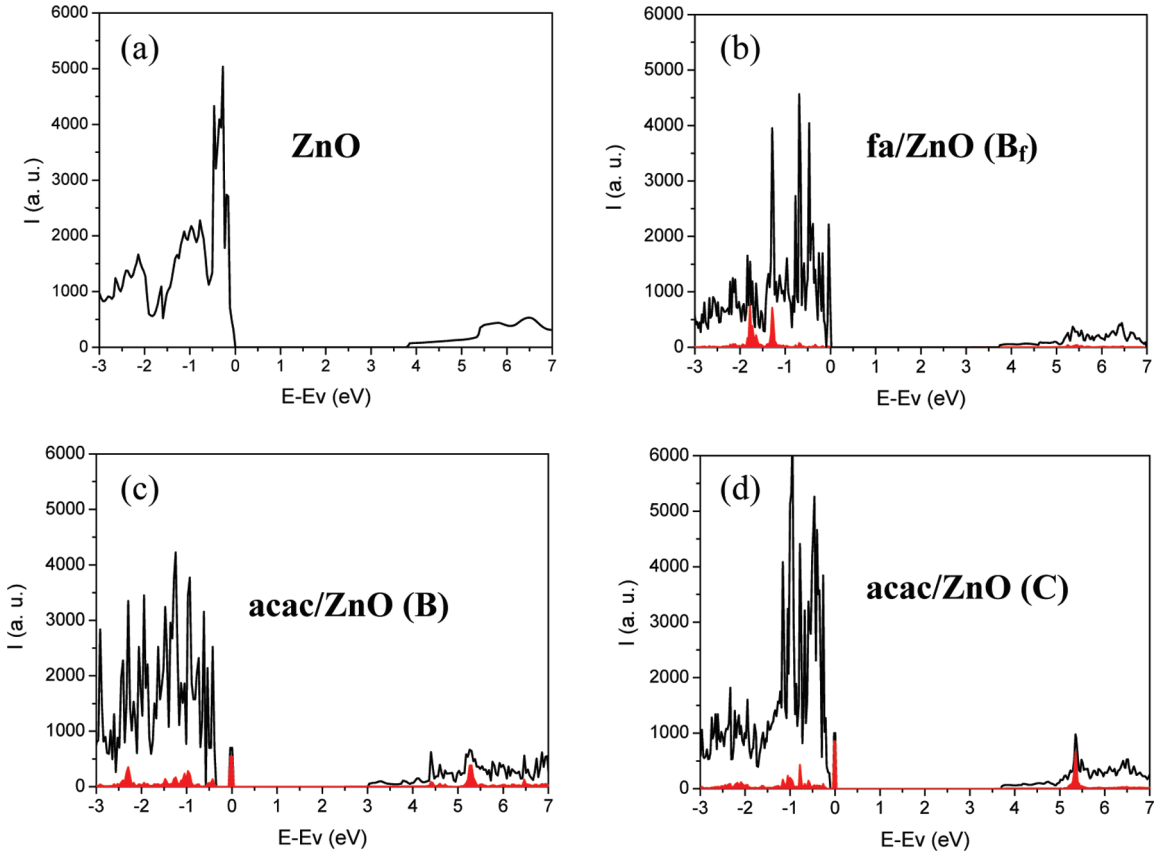

Figure 3. Total DOS (black) and projected DOS on the molecule (red) computed for (a) a free ZnO(10−10) surface, (b) for a **fa**/ZnO system (B_f mode), and for a **acac**/ZnO system for a B mode (c) and a C mode (d).

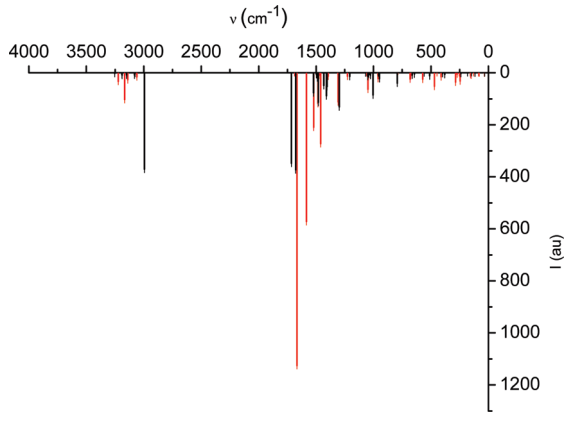

Figure 4. IR spectra of **acacH** (black) and Zn(**acac**)$_2$ (red) using SB computed in the gas phase.

formation will not be quantitatively satisfactory. Analogously, the Zn−O stretching is occurring in the same spectral region (below 500 cm^{-1}) as the vibrations belonging to the ZnO lattice. We expect that this vibration could thus not be used to detect the interaction of **acacH** and ZnO.

On the other hand, the shift of the most intense vibrations in the 1700−1500 cm^{-1} region seems better suited to follow the **acac** coordination to Zn or to a ZnO surface. In particular, going from the free **acacH** to the Zn(**acac**)$_2$ a shift from 1714 and 1676 cm^{-1} to 1650 and 1572 cm^{-1} is computed for the symmetric CO CC and the antisymmetric CO CC stretching vibrations, respectively. The computed absolute values—and shifts—compare well to the experimental values measured in gas phase, that is 1642 and 1624 cm^{-1} for **acacH**[50] to 1592 and 1523 cm^{-1} for Zn(**acac**)$_2$[44] (Table 2). Physically, the origin of the shift to lower energy upon coordination to the Zn atom is due both to a lengthening of the CO and CC bonds, due to the formation of the Zn−O bond, and to the absence of the intramolecular H

Table 2. Selected Computed and Experimental IR Frequencies of acacH, Zn(acac)$_2$, and acac/ZnO

		computed			experimental		
		acacH	Zn(**acac**)$_2$	**acac**/ZnO	**acacH**	Zn(**acac**)$_2$	**acac**/ZnO
OH		2995	--	--	2800−2900[c]	--	--
CO/CC stretching	ν_{sym}	1714	1650	1649[a]/1673[b]	1642[c]/1705[e]	1592[d]	1651[e]
	ν_{asym}	1676	1572	1575[a]/1575[b]	1624[c]/1624[e]	1523[d]	1604[e]

[a] Chelate mode. [b] Bidentate mode. [c] In vacuum from ref 50. [d] From ref 44. [e] In ethanol this work.

dx.doi.org/10.1021/la103634v |*Langmuir* 2011, 27, 3442–3450

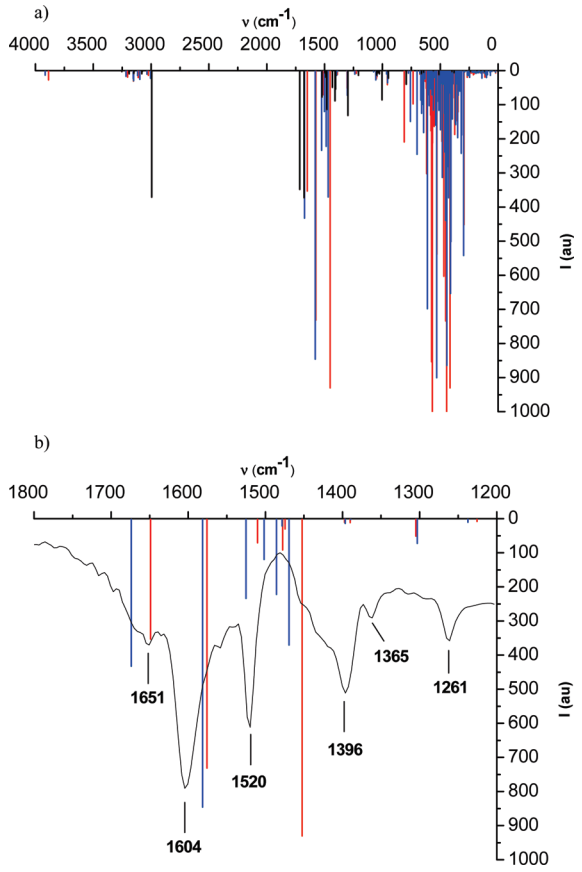

Figure 5. (a) Computed vibrations for the free **acacH** (black) compared with those of the **acac**/ZnO system in a chelate (red) and bidentate adsorption (blue) modes. (b) Experimental ATR-IR spectrum of the **acac**/ZnO system (black) compared to the computed **acac**/ZnO IR spectra of the chelate (red) and the bidentate (blue) adsorption modes.

bond that is stabilizing the **acacH** in its *cis* conformation through the formation of a six member pseudo-ring. In this respect, it is worth stressing that the vibrations computed for the free **acacH** molecule show also a large contribution of the OH stretching mode.

If the shift of CO and CC stretching vibrations could be used to monitor the coordination of the **acac** to the ZnO surface, it is still to be clarified if this shift will be sufficiently sensitive to the coordination mode to allow discriminating between chelate and bidentate adsorption modes.

To this end the spectra of the **acac** molecule adsorbed on the ZnO surface in a chelate and bidentate modes were computed and compared to the data computed for the free **acacH**. The results obtained are reported in Figure 5. It is worth noting that, to the best of our knowledge, no experimental data are available in the literature for the **acac**/ZnO system. For this reason the IR ATR spectra of **acacH** and **acac**/ZnO were experimentally recorded in the same conditions focusing on the spectral region between 1200 and 1800 cm^{-1}, that is of highest interest for CO and CC vibrations (Figure 5b and Figure S2, Supporting Information). Experimentally, we observed a shift of the symmetric and antisymmetric CO−CC stretching modes from 1705 and 1624 cm^{-1} to 1651 and 1604 cm^{-1} for **acacH** and **acac**/ZnO system respectively (table2, Figure S2, Supporting Information). The observed decreases in the transition energies of the CO−CC stretching mode are evidence of the **acac** adsorption on the ZnO surface.

These modes, computed around 1600 cm^{-1}, are indeed shifted to lower energies upon adsorption of the **acacH** on the surface, in analogy with the Zn(**acac**)$_2$ complex (Figure 5a and Table 2). Unfortunately, these IR frequencies are not significantly different for the chelate (1649 and 1575 cm^{-1}) and bidentate (1673 and 1575 cm^{-1}) adsorption modes. These frequencies are related to local vibrations directly related to the C−O distance which is probably poorly affected by the presence of surrounding molecules such as coadsorbed solvent molecules and other **acac** molecules. It is also important to stress that the description of the overall adsorption mechanism and of the properties of adsorbed molecules would definitely need a correct treatment of solvent effects (presence of coadsorbed solvent molecules, first solvation shell of the molecule). Nevertheless for the time being a proper description of solvent effects for extended systems at ab initio level is far to be defined and most of the studies neglect this effect.[51−53]

Moreover, from our calculations it is clear that the spectral region around 500 cm^{-1} cannot be used to follow adsorption since all lattice vibrations occur in this region (Figure 5a). Therefore, we can conclude that IR spectroscopy can be suitable to follow adsorption on surface but that it will probably not allow to discriminate between the different adsorption modes.

IV. CONCLUSION

Seeking for a rational design of new anchoring groups for hybrid materials, two different and stable adsorption modes for the acetylacetone molecule on a ZnO(10−10) surface, namely a bidentate and a chelating modes, were investigated by means of a periodic DFT approach, using a hybrid functional (PBE0).

Both adsorption modes are dissociative and the computed adsorption energies are of the same order of magnitude as those found, at the same level of theory, for the most stable adsorption mode of formic acid on ZnO, this latter being taken as a prototype for carboxylate anchoring groups.

Indeed, the overall orientation of the **acac** molecule, which in both case is found to be bent toward the surface, is governed by hydrogen bonds between the **acac** and oxygen atoms of the surface. From an electronic point of view, the acetylacetone contributes strongly to the valence band of the system but only slightly to the conduction band.

Then, from the analysis of the computed IR spectra it seems possible to follow the adsorption of **acacH** on the ZnO surface by inspection of the energetic shift of the most intense CO and CC stretching bands of the IR spectra although these latter will not be sufficiently sensitive to distinguish between a chelate and bidentate adsorption mode.

In summary, according to our theoretical and experimental findings, the acetylacetone chemical group appears as very promising for ZnO functionalizing and for developing new hybrid materials for advanced applications. This anchoring group, found to be as good as carboxylic acid (high adsorption energy) without the drawback of presenting a rather strong acidity, should not lead to pronounced morphological modifications upon grafting. Clearly the overall efficiency of a hybrid system will depend on the coupling between the entire molecule and the substrate. In this respect, this study represents only a first step toward the design of new efficient devices based on the use of anchoring group combining a high adsorption energy with

a controlled orientation of the molecule with respect to the surface.

■ ASSOCIATED CONTENT

Supporting Information. Computed IR frequencies for the free **acacH** and Zn(**acac**)$_2$ systems using the SB and LB; measured ATR-IR (transmission) of **acacH** in ethanol and **acac**/ZnO; geometries, DOS and IR wavenumber of the CC and CO stretching computed for the Bf, B and C systems taking into account the dispersion corrections through the Grimme scheme; isosurfaces of the localized orbital computed inside the ZnO gap for the B and C adsorption modes; and structural and energetic features computed for an eight atomic planes acac/ZnO system. This material is available free of charge via the Internet at http://pubs.acs.org.

■ AUTHOR INFORMATION

Corresponding Author

*E-mail: (T.L.B.) tangui-le-bahers@chimie-paristech.fr; (I.C.) ilaria-ciofini@chimie-paristech.fr.

■ ACKNOWLEDGMENT

Prof. Carlo Adamo, Dr. Philippe P. Lainé and Dr. Anouk Galtayries are thanked for fruitful discussions. The French National Agency for Research (ANR) is acknowledged for financial support to I.C. in the framework of the "NEXUS project (Programme Blanc 2007, BLAN07-1-196405) and to T.P. and I. C. in the framework of the Asyscol project (Programme Habitat intelligent et solaire photovoltaïque 2008, ANR-08-HABISOL-002).

■ REFERENCES

(1) Yoshida, T.; Minoura, H.; Zhang, J.; Komatsu, D.; Sawatani, S.; Pauporté, T.; Lincot, D.; Oekermann, T.; Schlettwein, D.; Tada, H.; Wöhrle, D.; Funabiki, K.; Matsui, M.; Miura, H.; Yanagi, H. *Adv. Funct. Mater.* **2009**, *19*, 17–43.

(2) Badre, C.; Pauporté, T.; Turmine, M.; Lincot, D. *Nanotechnology* **2007**, *18*, 365705.

(3) Badre, C.; Pauporté, T. *Adv. Mater.* **2009**, *21*, 697–701.

(4) Lupan, O.; Guérin, V. M.; Tiginyanu, I. M.; Ursaki, V. V.; Chow, L.; Heinrich, H.; Pauporté, T. *J. Photochem. Photobiol. A: Chemistry* **2010**, *211*, 65–73.

(5) Irrera, S.; Costa, D.; Ogle, K.; Marcus, P. *Superlattices Microstruct.* **2009**, *46* (1−2), 19–24.

(6) Pauporté, T.; Bedioui, F.; Lincot, D. *J. Mater. Chem.* **2005**, *15*, 1552–1559.

(7) Pauporté, T.; Bataille, G.; Joulaud, L.; Vermersch, J. F. *J. Phys. Chem. C* **2010**, *114*, 194–202.

(8) Youngblood, W. J.; Anna Lee, S.-H.; Kobayashi, Y.; Hernandez-Pagan, E. A.; Hoertz, P. G.; Moore, T. A.; Moore, A. L.; Gust, D.; Mallouk, T. *J. Am. Chem. Soc.* **2009**, *131*, 926–927.

(9) Woolerton, T. W.; Sheard, S.; Reisner, E.; Pierce, E.; Ragsdale, S. W.; Armstrong, F. A. *J. Am. Chem. Soc.* **2010**, 132.

(10) Zhang, Q.; Dandeneau, C. S.; Zhou, X.; Cao, G. *Adv. Funct. Mater.* **2009**, *21*, 4087–4108.

(11) Pauporté, T. Toward Functional Nanomaterials, Chapter 2. In *Design of solution-grown ZnO nanostructures*;Wang Zhiming, M., Ed.; Lecture Notes in Nanoscale Science and Technology 5; , Springer: New York, 2009; pp 77−127.

(12) Horiuchi, H.; Katoh, R.; Hara, K.; Yanagida, M.; Murata, S.; Arakawa, H.; Tachiya, M. *J. Phys. Chem. B* **2003**, *107*, 2570–2574.

(13) Li, G.; Sproviero, E. M.; McNamara, W. R.; Snoeberger, R. C., III; Crabtree, R. H.; Brudvig, G. W.; Batista, V. S. *J. Phys. Chem. B* **2011**10.1021/jp908925z.

(14) Jiang, Y.; Wu, N.; Wu, H.; He, M. *Synlett* **2005**, 2731–2734.

(15) Olivier, J.-H.; Haefele, A.; Retailleau, P.; Ziessel, R. *Org. Lett.* **2010**, *12*, 1672–1675.

(16) McNamara, W. R.; Snoeberger, R. C., III; Li, G.; Schleicher, M.; Cady, C. W.; Poyatos, M.; Schmuttenmaer, C. A.; Crabtree, R. H.; Brudving, G. W.; Batista, V. S. *J. Am. Chem. Soc.* **2008**, *130*, 14329–14338.

(17) Saunders, V. R.; Dovesi, R.; Roetti, C.; Orlando, R.; Zicovich-Wilson, C. M.; Harrison, N. M.; Doll, K.; Civalleri, B.; Bush, I.; D'Arco, Ph.; Llunell, M. *Crystal 06 User's Manual*; Universita di Torino: Torino, Italy, 2006.

(18) Pauporté, T.; Rathousky, J. *J. Phys. Chem. C* **2007**, *111*, 7639–7644.

(19) Dovesi, R.; Civalleri, B.; Orlando, R.; Roetti, C. Saunders, V. R. *Ab Initio Quantum Simulation in Solid State Chemistry*; Lipkowitz, K. B., . Larter, R., Cundari, T. R., Eds.; Reviews in Computational Chemistry 21; Wiley-VCH: New York, 2005; pp 1−125.

(20) Labat, F.; Ciofini, I.; Hratchian, H. P.; Firsch, M.; Raghavachari, K.; Adamo, C. *J. Am. Chem. Soc.* **2009**, *131*, 14290–14298.

(21) Labat, F.; Ciofini, I.; Adamo, C. *J. Chem. Phys.* **2009**, *131*, 044708.

(22) Barthelat, J.-C.; Durand, P. *Gazz. Chim. Ital.* **1978**, *108*, 225.

(23) Barthelat, J.-C.; Durand, P.; Serafini, A. *Mol. Phys.* **1977**, *33*, 159.

(24) Hay, P. J.; Wadt, W. R. *J. Chem. Phys.* **1985**, *82*, 284.

(25) Adamo, C.; Barone, V. *J. Chem. Phys.* **1999**, *110*, 6158.

(26) Perdew, J. P.; Burke, K.; Ernzerhof, M. *Phys. Rev. Lett.* **1996**, *77*, 3865–3868.

(27) Meyer, B.; Marx, D. *Phys. Rev. B* **2003**, *67*, 035403.

(28) Boys, S. F.; Bernardi, F. *Mol. Phys.* **1970**, *19*, 553.

(29) Pascale, F.; Zicovich-Wilson, C. M.; Lopez, F.; Civalleri, B.; Orlando, R.; Dovesi, R. *J. Comput. Chem.* **2004**, *25*, 888–897.

(30) Zicovich-Wilson, C. M.; Pascale, F.; Roetti, C.; Saunders, V. R.; Orlando, R.; Dovesi, R. *J. Comput. Chem.* **2004**, *25*, 1873–1881.

(31) Total energy calculation were performed with a convergence criteria of 10^{-10} Ha (TOLDEE parameter fixed to 10).

(32) Grimme, S. *J. Comput. Chem.* **2006**, *27*, 1787–1799.

(33) Saunders, V. R.; Dovesi, R.; Roetti, C.; Orlando, R.; Zicovich-Wilson, C. M.; Harrison, N. M.; Doll, K.; Civalleri, B.; Bush, I.; D'Arco, Ph.; Llunell, M. *Crystal 09 User's Manual*; Universita di Torino: Torino, Italy, 2009.

(34) Dovesi, R.; Orlando, R.; Civalleri, B.; Roetti, R.; Saunders, V. R.; Zicovich-Wilson, C. M. *Z. Kristallogr.* **2005**, *220*, 571–573.

(35) Gaussian 09, Revision A.02, Frisch, M. J.; Trucks, G. W.; Schlegel, H. B.; Scuseria, G. E.; Robb, M. A.; Cheeseman, J. R.; Scalmani, G.; Barone, V.; Mennucci, B.; Petersson, G. A.; Nakatsuji, H.; Caricato, M.; Li, X.; Hratchian, H. P.; Izmaylov, A. F.; Bloino, J.; Zheng, G.; Sonnenberg, J. L.; Hada, M.; Ehara, M.; Toyota, K.; Fukuda, R.; Hasegawa, J.; Ishida, M.; Nakajima, T.; Honda, Y.; Kitao, O.; Nakai, H.; Vreven, T.; Montgomery, Jr., J. A.; Peralta, J. E.; Ogliaro, F.; Bearpark, M.; Heyd, J. J.; Brothers, E.; Kudin, K. N.; Staroverov, V. N.; Kobayashi, R.; Normand, J.; Raghavachari, K.; Rendell, A.; Burant, J. C.; Iyengar, S. S.; Tomasi, J.; Cossi, M.; Rega, N.; Millam, N. J.; Klene, M.; Knox, J. E.; Cross, J. B.; Bakken, V.; Adamo, C.; Jaramillo, J.; Gomperts, R.; Stratmann, R. E.; Yazyev, O.; Austin, A. J.; Cammi, R.; Pomelli, C.; Ochterski, J. W.; Martin, R. L.; Morokuma, K.; Zakrzewski, V. G.; Voth, G. A.; Salvador, P.; Dannenberg, J. J.; Dapprich, S.; Daniels, A. D.; Farkas, Ö.; Foresman, J. B.; Ortiz, J. V.; Cioslowski, J.; Fox, D. J. Gaussian, Inc.: Wallingford CT, 2009.

(36) Ugiengo, P.; Pascale, F.; Mewara, B.; Labeguerie, P.; Tosoni, S.; Dovesi, R. *J. Phys. Chem. B* **2004**, *108*, 13632–13637.

(37) Pascale, F.; Tosoni, S.; Zicovich-Wilson, C. M.; Ugliengo, P.; Orlando, R.; Dovesi, S. *Chem. Phys. Lett.* **2004**, *396*, 4–6.

(38) Lefèvre, G. *Adv. Colloid. Interfa.* **2004**, *107*, 109.

(39) Persson, P.; Lunell, S.; Ojamäe, L. *Int. J. Quantum Chem.* **2002**, *89*, 172.

(40) Persson, P.; Ojamäe, L. *Chem. Phys. Lett.* **2000**, *321*, 302–308.
(41) Shao, X.; Fukui, K.-I.; Kondoh, H.; Shionoya, M.; Iwasawa, Y. *J. Phys. Chem. C* **2009**, *113*, 14356.
(42) Kosmulski, M. *Chemical Properties of Material Surfaces*; Marcel Dekker: New York, 2001.
(43) Antina, E. V.; Belova, N. V.; Berezin, M. B.; Girichev, G. V.; Giricheva, N. I.; Zakharov, A. Z.; Petrova, A. A.; Shlykov, S. A. *J. Struct.. Chem.* **2009**, *50*, 1035–1045.
(44) Massue, J.; Bellec, N.; Chopin, S.; Levillain, E.; Roisnel, T.; Clérac, R.; Lorcy, D. *Inorg. Chem.* **2005**, *44*, 8740–8748.
(45) Tamames, B.; Sousa, S. F.; Tamames, J.; Fernandes, P. A.; João Ramos, M. *Proteins* **2007**, *69*, 466–475.
(46) Le Bahers, T.; Pauporté, T.; Labat, F.; Ciofini, I. *Phys. Chem. Chem. Phys.* **2010**, *12*, 14710–14719.
(47) Schiffmann, F.; Hutter, J.; Vande Vondele, J. *J. Phys: Condens. Matter* **2008**, *20*, 064206.
(48) Lateral interaction energy is computed as $E_L = E_{Surf,Madsorbate} - E_{surf/adsorbate}$ where $E_{surf/adsorbate}$ is the energy of the isolated adsorbate frozen in its optimized structure on the surface, and $E_{Surf,Madsorbate}$ is the energy of a monolayer of adsorbates with the same periodicity as the surface cell.
(49) McNamara, W. R.; Snoeberger, R. C., III; Li, G.; Schleicher, J. M.; Cady, C. W.; Poyatos, M.; Schmuttenmaer, C. A.; Crabtree, R. H.; Brudvig, G. W.; Batista, V. S. *J. Am. Chem. Soc.* **2008**, *130*, 14329–14338.
(50) Tayyari, S.-F.; Milani-Nejad, F. *Spectrochim. Acta, Part A* **2000**, *56*, 2679–2691.
(51) Persson, P.; Ojamäe, L. *Chem. Phys. Lett.* **2000**, *321*, 302–308.
(52) Hirva, P.; Haukka, M. *Langmuir* **2010**, *26*, 17075–17081.
(53) Nilsing, M.; Persson, P.; Lunell, S.; Ojamäe, L. *J. Phys. Chem. C* **2007**, *111*, 12116–12123.